ELSEVIER

Computational Materials Science 19 (2000) 189–204

COMPUTATIONAL MATERIALS SCIENCE

www.elsevier.com/locate/commatsci

Modeling the mechanical behavior of a multicrystalline zinc coating on a hot-dip galvanized steel sheet

R. Parisot [a,b,*], S. Forest [a], A.-F. Gourgues [a], A. Pineau [a], D. Mareuse [b]

[a] *Laboratoire de métallurgie mécanique, UMR CNRS 7633, Centre des Matériaux, Ecole des Mines de Paris, BP 87-91003, Evry cedex, France*

[b] *CED, Usinor Recherche et Développement, 1 route de St-Leu, BP 39109, 60761 Montataire, France*

Abstract

Numerical simulations can play a major role in the understanding of deformation mechanisms in zinc coatings of galvanized steel sheets during forming processes. A three-dimensional finite element (FE) simulation of a thin zinc coating on a galvanized steel sheet has been performed taking the multicrystalline structure of the coating into account. Experimental characterization of the gauge length of a real in situ tensile specimen reveals 34 large flat zinc grains; the grain orientations are determined using the electron back-scatter diffraction (EBSD) technique. The geometry and orientation of the grains and the plastic deformation modes specific to hexagonal close-packed (hcp) metals as plastic slip and twinning are incorporated into the modeling using a classical crystal plasticity framework. The constraint effect of the substrate is evidenced by comparing the results to the computation of a zinc layer without substrate under the same loading conditions. Attention is then focused on, respectively, the initiation of plastic activity at the grain boundaries, the multiaxial stress state of the grains, the development of a strain gradient within the thickness. © 2000 Elsevier Science B.V. All rights reserved.

Keywords: Coating; Crystal plasticity; Finite element method; Galvanized steel; Hexagonal close-packed metal; Multicrystal; Zinc

1. Introduction

Zinc-based coatings are largely used for protection against corrosion of steel-sheet products in the automotive industry [1]. During stamping of galvanized steel sheet, the zinc coating undergoes large strain without significant damage. Recent works [2,3], including expansion tests for simulating stamping processes, investigated the damage modes of hot-dip galvanized steel sheets.

On one hand, mechanical properties of zinc coatings are strongly not the function of alloying elements and impurities, and since processing of hot-dip galvanization has been improved in the last five years, investigations are again necessary for the understanding of their mechanical behavior. On the other hand, polycrystal finite element (FE) simulations have been applied for bulk materials whereas dislocations models are proposed for coated materials [4]. In the literature, most of the polycrystal FE works deal with

* Corresponding author.
E-mail addresses: rodolphe.parisot@mat.ensmp.fr (R. Parisot), samuel.forest@mat.ensmp.fr (S. Forest).

0927-0256/00/$ - see front matter © 2000 Elsevier Science B.V. All rights reserved.
PII: S0927-0256(00)00155-5

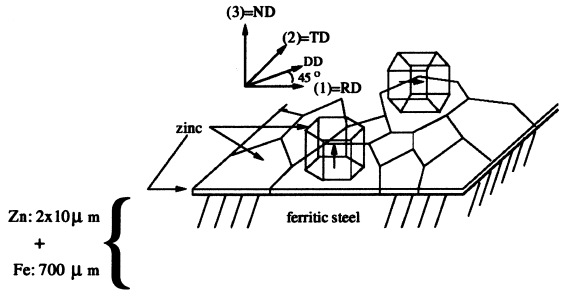

Fig. 1. Schematic microstructure of the zinc coating of the studied galvanized steel sheet. RD ≡ rolling direction, TD ≡ transverse direction and ND ≡ normal direction.

large strains [5]. These 2-D and quasi-3-D computations generally concern texture evolution of polycrystals and are compared with the classical approaches as the Taylor model. However, other considerations lead to original computations: e.g., Becker investigated the surface roughening during sheet forming [6] using 2-D computations. These computations generally do not take into account anisotropic effects of hardening in deformation modes assuming that all slip systems harden identically within the crystal [7]. More recently, Staroselsky and Anand studied law stacking fault energy fcc materials which deform by slip and twinning, introducing a twin resistance [8].

The aim of this work is to model the mechanical behavior of a hot-dip galvanized steel sheet supplied by USINOR. The zinc deposition process leads to a coating made of very flat zinc grains, with only one grain through the thickness, on a comparatively small-grained ferritic steel. Fig. 1 shows a schematic microstructure of such a coating. [1] The diversity of the deformation mechanisms taking place in zinc grains during overall tensile strain is presented: non-basal slip, twinning and strain relaxation at grain boundaries have been experimentally observed in this study. The individual grain orientations and the crystallographic texture of the coating are known using electron back-scatter diffraction (EBSD). Most grains have their ***c*** axis normal to the steel sheet and the other parallel to the sheet plane. As a result, three main components, deduced from careful microstructural observations, are required for a realistic simulation the deformation of zinc coatings:

- a model of the coating as a flat multicrystalline material taking individual grains into account;
- a 3-D representation of geometry of the specimen and of the mechanical deformation modes, namely the different slip system families;
- a sufficiently fine mesh to account for strong strain gradients in each grain and possibly through the thickness.

A first attempt to meet these requirements is presented in this work. The main advantage of the numerical approach accompanying a systematic experimental approach of the deformation mechanisms is the access to mechanical and physical quantities that are experimentally out of reach: multiaxial stress state in the grains, principal stresses near grain boundaries and near the interface, strain gradient through the thickness ...

FE simulations have been performed to describe the mechanical behavior of the zinc grains of an in situ tensile specimen previously characterized by light microscopy and EBSD. 34 individual zinc grains are considered as explained in Section 3. The constitutive equations for single crystals are based on classical crystal plasticity relying on Schmid law. Basal, prismatic and pyramidal slip systems have been considered

[1] Galvanizing bath is alloyed with aluminium to avoid the formation of brittle FeZn compounds, and to build the intermetallic Fe_2Al_5 ultra-thin layer at the interface. This layer is not taken into account in this work.

Table 1
Chemical composition of substrate (A, $\times 10^{-3}$ (wt%)) and coating (B, (wt%))

C	Mn	P	S	Al	Ni	Ti	Si
A							
1.7	134	12	8	45	14	55	19
Zn	Fe	Al					
B							
9.8	0.001	0.2					

together with a representation of twinning. As indicated in Table 1, the coating is not made of pure zinc. The mechanical properties of alloyed zinc are deduced from a systematic review of literature data reported in Section 2. In this work, it is assumed that the properties of bulk pure or alloyed zinc can be used for a thin layer: size and constraint effects are excluded in this first step. The substrate is regarded as a homogeneous elastoplastic material obeying Hill's criterion. The main results and new insights brought by the simulation are presented in Section 4.

2. Mechanical behavior of single crystalline zinc

2.1. Crystallographic elements and deformation mechanisms

Hexagonal close-packed (hcp) metal single crystals are characterized by the ratio (c/a) where c and a are the height and the edge size of the hexagonal cell, respectively. They are known to exhibit a very anisotropic mechanical behavior (both elasticity and plasicity). For zinc, $(c/a) = 1.856 > 1.633$ which is the value for maximal density of hcp metals. Therefore, basal slip is the easiest deformation mode in zinc [9,10]. Fig. 2 presents the slip systems of zinc in the hexagonal cell. To activate non-basal slip systems, the crystal must be loaded perpendicular or parallel to the basal plane. Bell and Cahn [11] were the first to identify pyramidal π_2 slip and measured a critical resolved shear stress (CRSS) 30 times greater than for basal slip. Table 2 indicates the crystallographic elements of the operative slip systems in zinc. Twinning can be considered as a slip system with two conditions: the Schmid law is applied for the growth of twins and not for nucleation

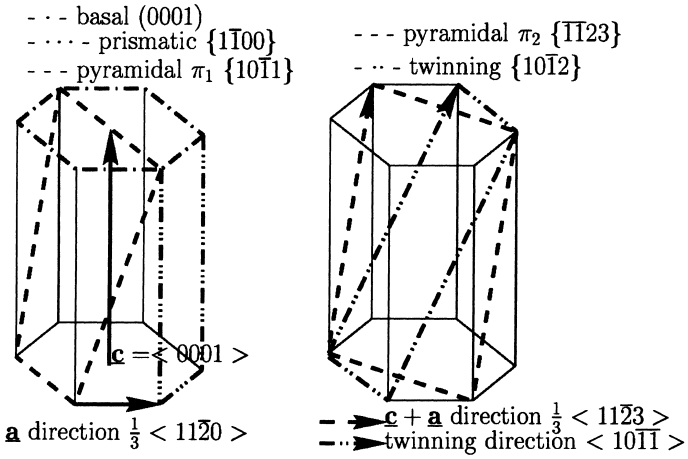

Fig. 2. Slip systems and twinning system of zinc.

Table 2
Deformation modes of zinc. $\Lambda = \sqrt{2/3}(c/a)$

Direction	Plane	Crystallographic elements	Frank indexation [12]	Number of systems
$\boldsymbol{a}$	Basal	$(0001)\langle 11\bar{2}0\rangle$	$(000\,\frac{1}{\Lambda})\langle 11\bar{2}0\rangle$	3
$\boldsymbol{a}$	Prismatic	$\{1\bar{1}00\}\langle 11\bar{2}0\rangle$	$\{1\bar{1}00\}\langle 11\bar{2}0\rangle$	3
$\boldsymbol{a}+\boldsymbol{c}$	Pyramidal π_2	$\{11\overline{22}\}\langle\overline{11}23\rangle$	$\{11\bar{1}\,\frac{2}{\Lambda}\}\langle\overline{11}2(3\Lambda)\rangle$	6
	Twinning	$\{10\bar{1}2\}\langle 10\overline{11}\rangle$	$\{10\bar{1}\,\frac{2}{\Lambda}\}\langle 10\bar{0}(\bar{1}\Lambda)\rangle$	6

(i.e., $\tau_c^{\text{twin}} \equiv \tau_{\text{growth}_c}^{\text{twin}}$) and the twinning has to obey the non-symmetrical condition $\tau^{\text{twin}} - \tau_c^{\text{twin}} > 0$ to be activated. Crystallographic elements of slip systems are given in classical indexation for hcp metals with four indices.

Some deformation modes of the coating have been identified by experiments: basal and non-basal slips have been observed as well as twinning and strain relaxation at grain boundaries.

2.2. Identification of material parameters for zinc single crystals at room temperature

The elastic anisotropy of zinc single crystal is taken into account: the stiffness tensor $\underset{\approx}{\boldsymbol{E}}$ used for calculation is: $E_{1111} = 165$ GPa, $E_{2222} = 165$ GPa, $E_{3333} = 61.8$ GPa, $E_{1212} = 66.95$ GPa, $E_{2323} = 39.6$ GPa, $E_{3131} = 39.6$ GPa, $E_{1122} = 31.1$ GPa, $E_{2233} = 50$ GPa, $E_{3311} = 50$ GPa.

2.2.1. Identification of the CRSS of slip systems of pure zinc

The values of critical resolved shear stress (CRSS) of basal systems in zinc from literature data are very scattered. Compression tests [13], tension tests [11] and simple shear tests [14] have been performed on pure and alloyed zinc single crystal. It was found for CRSS of basal slip systems in pure zinc, respectively: 0.1, 0.3 and 0.5 MPa.

A similar debate exists for pyramidal π_2 slip systems. Stofel and Wood [10] performed tension/torsion tests and studied latent hardening between basal system and pyramidal π_2 systems. When no basal slip has occurred before pyramidal slip is activated, they found a CRSS for π_2 to be $\tau_c^{\pi_2} = 3$ MPa. Bell and Cahn [11] and Fundenberger et al. [15] found, respectively, 10–15 MPa and $\tau_c^{\pi_2}/\tau_c^{\text{bas}} = 10$, the latter after identification of texture evolution of cold-rolled zinc using a Taylor model. Very few papers deal with prismatic slip. Only [15] have identified a CRSS for prismatic slip. They found $\tau_c^{p}/\tau_c^{\text{bas}} = 15$, which is the value used here for simulations.

Twinning is a complex phenomenon including nucleation and growth processes. Twin nucleation occurs in a region where local stress concentrations take place. Although the mechanisms of twin growth are still controversial, it is commonly admitted that it can be described by a Schmid law. An initial CRSS $\tau_c^{\text{twin}} = 5$ MPa is realistic.

2.2.2. Solution hardening effects of additional elements

As mentioned in the introduction, the galvanization bath is alloyed with aluminium to avoid brittle ZnFe compounds. The chemical analysis reveals the composition (Zn + 0.2(wt%)Al) in the coating. Adams and Vreeland [13] studied pure zinc and two zinc alloys: (Zn + 0.0025(wt%)Al) and (Zn + 0.02(wt%)Al). The last is the closest composition, to the coating one, obtained from the literature. They found that the CRSS of basal system increases from 0.1 MPa for pure zinc to 0.5 MPa for (Zn + 0.02(wt%)Al). In contrast, they found latent hardening of the basal slip to be independent of Al concentration. CRSS values of alloyed zinc present in the coating are summarized in Table 3. Accordingly, the influence of solution hardening for the

Table 3
CRSS used for Zn + 0.2(wt%)Al for finite element simulations from [13]

Slip family	Basal	Pyramidal π_2	Prismatic	Twinning
CRSS (MPa)	1,5	15	22,5	25

composition of the coating considered in this work leads to a correction of the values given in paragraph Section 2.2 for pure zinc by a factor of about five.

2.2.3. Identification of hardening

The identification of slip systems observed experimentally indicate that deformation mechanisms of zinc coating on hot-dip galvanized steel sheet include non-basal slip. This implies that the interaction between slip systems and slip systems families, including self and latent hardening must be taken into account. The hardening law (i.e., the evolution of CRSS with plastic slip) and the literature review of hardening of zinc are given in the appendix.

Stofel and Wood [10] and Bosin et al. [14] found the self hardening of basal systems and the latent hardening to be anisotropic. This anisotropy has been taken into account in the modeling of the mechanical behavior of zinc single crystal.

Identification of viscosity parameters Zinc has a low melting point, $T_m = 419°C$, and at room temperature, $(T/T_m) = 0.43$. Therefore, it is necessary to model the rate-dependent behavior of zinc. This was done using a Norton-type viscoplastic law with threshold to compute the slip rate of system s:

$$\begin{cases} \dot{\gamma}^s = \mathrm{Max}\left(0, \left((|\tau^s| - \tau_c^s)/K\right)^n\right)\mathrm{sign}(\tau^s), \\ \dot{\gamma}^s_{\mathrm{cum}} = |\dot{\gamma}^s|. \end{cases} \tag{1}$$

Compression tests on zinc single crystals at various strain rates have been performed by Mikulowski [16]. Parameters $(K,\ n)$ have been derived from their results and compared with Stahl and Margolin works [17]: $K = 10$ MPa $s^{1/n}, n = 0.1$.

3. Experimental analysis of a multicrystalline coated steel sheet specimen

The geometry of an in situ tensile specimen of galvanized sheet, tested in the scanning electron microscope (SEM) chamber is given in Fig. 3. Attention is focused on a central area of 3.7 mm (length) × 1.5 mm (width).

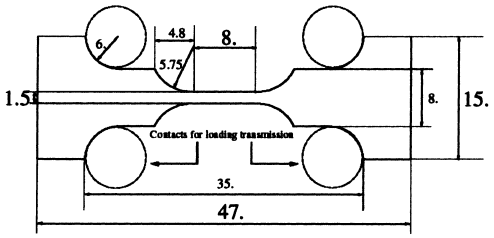

Fig. 3. In situ tensile specimen geometry. Thickness = sheet thickness (0.7 mm).

3.1. The substrate

The interstitial free steel substrate exhibits a homogeneous slightly orthotropic mechanical behavior. The identification of the mechanical behavior was performed using tensile tests with large strain gauges in rolling direction (RD), transverse direction (TD) and diagonal direction (DD) at 45° of the RD direction. The coating of tensile specimen was previously dissolved. The mechanical behavior of the substrate is modeled using a Hill criterion and a non-linear hardening law:

$$f(\underset{\sim}{\boldsymbol{\sigma}}, R) = \underset{\sim}{\boldsymbol{s}} : \underset{\approx}{\boldsymbol{H}} : \underset{\sim}{\boldsymbol{s}} - R^2 = as_{11}^2 + bs_{22}^2 + cs_{33}^2 + 2\left(ds_{12}^2 + es_{23}^2 + fs_{31}^2\right) - R^2 \tag{2}$$

$$R = R_0 + Q_1\left(1 - e^{(-b_1 p)}\right) + Q_2\left(1 - e^{(-b_2 p)}\right), \tag{3}$$

where the reference $(1,\ 2,\ 3) \equiv (RD,\ TD,\ ND)$ and where $\underset{\sim}{\boldsymbol{s}}$ is the deviatoric stress tensor. In the present case, only the a, b, c and d parameters are stimulated. The identification process has led to the following set of parameters:

$$\begin{cases} a = 1.105, \quad b = 1.126, \quad c = 1, \quad d = 1.080 \\ R_0 = 107 \text{ MPa}, \quad Q_1 = 171 \text{ MPa}, \quad b_1 = 19, \\ Q_2 = 60 \text{ MPa}, \quad b_2 = 36. \end{cases} \tag{4}$$

Fig. 4 gives the comparison between the experiments and the simulations for rolling and transverse directions.

3.2. The coating

The low thickness of the zinc coating prohibits mechanical polishing. The tensile specimen has been electropolished using C_1 bath [18] with an imposed tension of 30 V. Note that this polishing does not reduce the roughness of the specimen. Fig. 5 shows the microstructure of the specimen observed using a polarized light microscope.

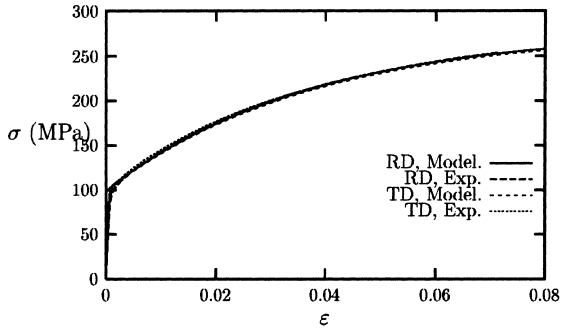

Fig. 4. Simulations vs. experiments for the substrate in RD and TD directions.

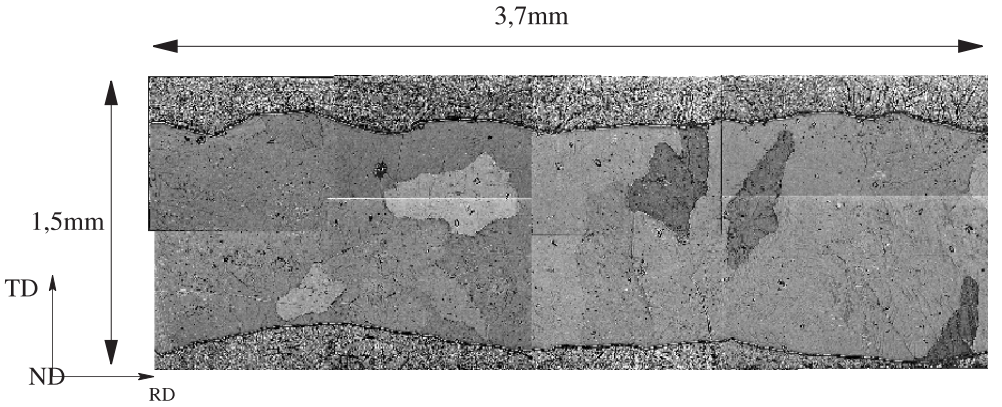

Fig. 5. Microstructural analysis of an in situ tensile specimen. Polarized light micrography. Non-polished areas are due to varnish applied on the ferritic steel to avoid local electrochemical reactions.

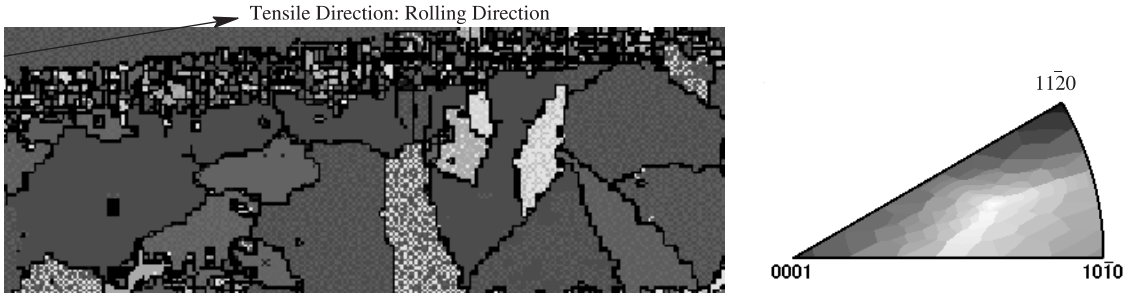

Fig. 6. EBSD analysis of an in situ tensile specimen together with the inverse pole figure.

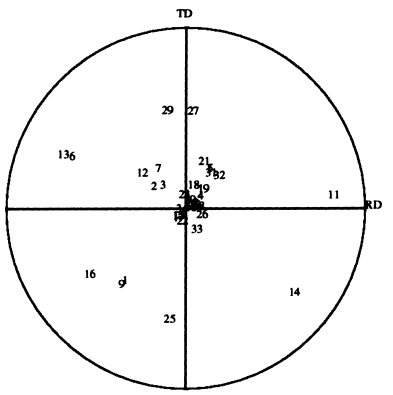

Fig. 7. Stereographic projection of the (0 0 0 1) poles of grains of the finite element mesh. The numbers refer to the FE mesh Fig. 8.

An EBSD analysis was performed on the same part of the in situ tensile specimen. Fig. 6 presents the map of orientations in the considered area. This analysis provides the Euler angles for each grain. Fig. 7 shows the (0 0 0 1) pole figure of these grains. Most of the grains have their ***c*** axis almost normal to the sheet plane; only 10 grains are strongly disoriented. Numbers refer to the FE mesh of Fig. 8.

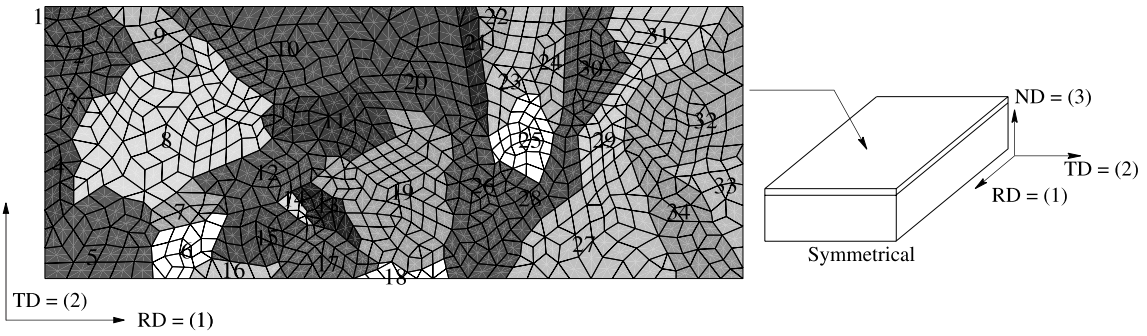

Fig. 8. Finite element mesh of the experimentally tested tensile specimen.

The sample of Fig. 3 was then tested in tension in a SEM chamber. The results are reported in Section 4.7 and compared with the numerical simulation.

4. FE analysis of a coated steel sheet

4.1. 3-D FE mesh and boundary conditions

The 2-D FE mesh of Fig. 8 including 1029 elements, was deduced from the previous observations. 34 sets of elements are distinguished to represent the 34 grains of the specimen. A 3-D mesh is obtained by translation of the 2-D mesh in the normal direction (ND), assuming that the planes of grain boundaries are perpendicular to the sheet plane, which is not far from being true for the present microstructure. Four layers are piled up for meshing the coating in the thickness while only one layer is used for meshing the thickness of the substrate. The 3-D mesh is made of 5145 bricks which corresponds to 37 170 (reduced) integration points with 22 165 nodes for quadratic elements and 5646 nodes for linear elements.

The following boundary conditions have been applied in order to simulate tension in direction (RD):

- Displacement $\boldsymbol{U}_3 = 0$ on the mid steel plane $(x_1,\ x_2)$.
- Displacement $\boldsymbol{U}_1$ is prescribed on the two end planes $(x_2,\ x_3)$.
- Other planes are left free of forces.

The computation has been carried out up to 2% macroscopic strain, which leads to significantly higher local strains. The same computation has been considered for a zinc film, without substrate, using otherwise the same boundary conditions.

4.2. Mesh sensitivity

The three-dimensional character of the computation and the strongly non-linear constitutive behavior of the grains lead to very long computation times (several weeks of CPU time). The number of elements was kept small enough for the computation to be performed on a workstation. However, this number is still too small to have a fully converged FE approximation: non-negligible differences can be noticed locally between the results using quadratic or linear elements. Linear elements lead to stiffer local responses and strain localization phenomena are delayed and alleviated in comparison to the quadratic approximation. However, the precision reached using this mesh is sufficient to capture several aspects of the deformation of coated materials. The use of finer meshes will require parallel computing.

4.3. Activated slip systems – strain localization

After $E_{11} = 1\%$ macroscopic strain, the local strain ε_{11} remains relatively homogeneous in each grain and is controlled by the underlying substrate: ε_{11} values vary from 0.003 to 0.02 and maxima are localized at grain boundaries. However, plastic strain turns out to be heterogeneous from grain to grain. Fig. 9 shows the plastic strain due to all deformation modes. As expected, the plastic strain due to basal slip γ_{eq}^{bas} is much greater than plastic strain due to non-basal slip. Fig. 9(a) shows that some grains are strongly plastically deformed (up to 10% of basal plastic strain) whereas other grains deform mainly elastically. Non-basal slip is essentially observed in the vicinity of grain boundaries. This is due to stress concentrations arising at grain boundaries.

4.4. Strain gradient through the coating

Fig. 10 shows basal plastic slip at different sections through the coating. Except for two grains (8 and 28) which are plastically deformed at free surface and not at the interface, most of the grains do not exhibit a strong strain gradient within the thickness. The thickness of the coating seems to be too small for a strain gradient from the interface to the free surface to develop at least at the investigated overall strain.

4.5. Influence of the substrate

The best way to evidence the influence of the substrate on the strain of the zinc layer is to compare the strain of the coating with the strain of a single zinc layer, i.e., without substrate. While such a test on a thin layer remains a challenge, the test can be simulated numerically. The two sides of the layers are free of forces. In Fig. 11, three maps of plastic strain due to basal slip are shown at macroscopic strain $E_{11} = 0.05\%$. The first is concerned with the strain of the zinc layer with an appropriate color scale called A. The second map represents the basal slip in the case substrate + coating for the same overall strain and with the same colors scale. The third map is the same as the second one but with a more appropriate color scale called B. Comparison of the first two maps shows that, without substrate, the strain of zinc grains is much more localized than with a substrate. In contrast, strain in the coating is almost prescribed by the substrate. This implies that strain of zinc grains is much more homogeneous. The mean strain state for each zinc grain of the substrate + coating system corresponds to a usual tension state. The associated stress state is multiaxial as explained below. Furthermore, comparison of the first and third maps shows that the most deformed grains are not the same. Activated slip systems within the zinc grains are even not the same with or without a substrate. This is due to the completely different stress state in each grain.

It is interesting to focus our attention on the strain and stress tensors of a particular grain, grain 11 of Fig. 8, and to simulate a tension test on a single crystal of zinc having the same orientation. For tension in direction 1, this single crystal exhibits the following plastic strain state:

$$\underset{\sim}{\boldsymbol{\varepsilon}}^{p}_{\chi^{11}} \simeq \begin{bmatrix} \varepsilon^{p} & 0 & 0 \\ 0 & 0 & 0 \\ 0 & 0 & -\varepsilon^{p} \end{bmatrix}, \tag{5}$$

where χ^{11} means single crystal oriented like grain 11. The reason is that only one basal slip system is activated during the test, with its slip direction in the plane (RD, ND). But the substrate tends to impose a tensile strain state to the zinc grain of the form $\underset{\sim}{\boldsymbol{\varepsilon}}^{p}_{\text{sheet}}$, which inevitably results in a strongly biaxial mean stress:

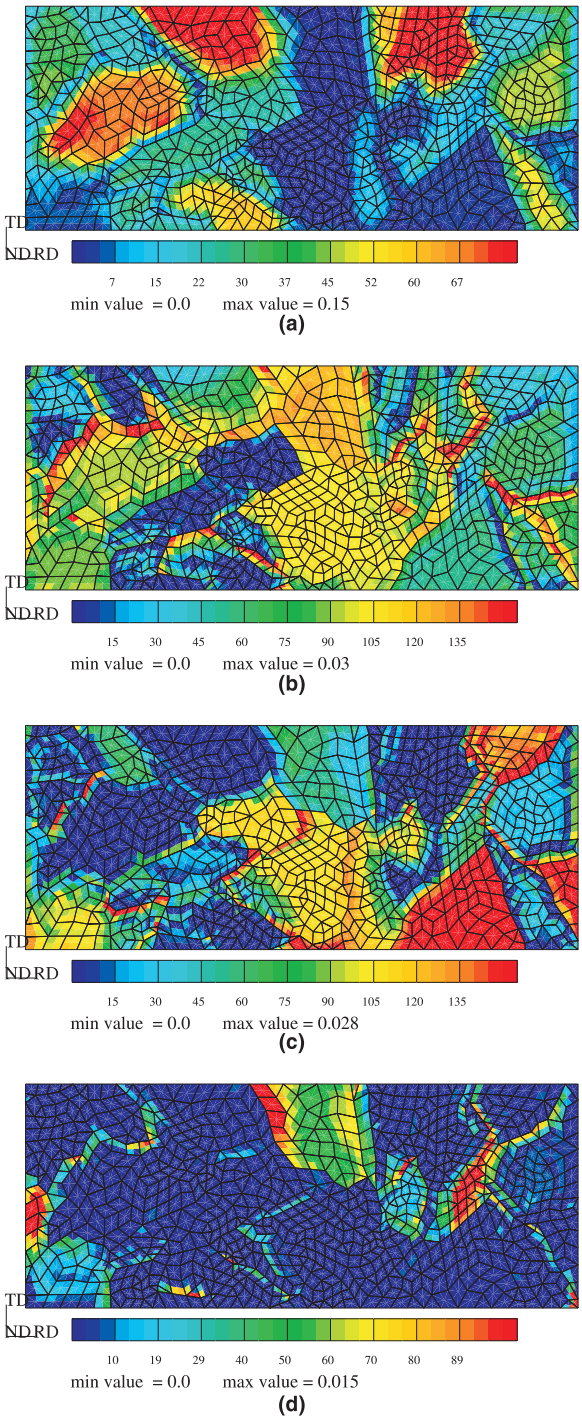

Fig. 9. Plastic strain due to different slip systems at free surface: (a) basal slip systems; (b) prismatic slip systems; (c) pyramidal π_2 slip systems and (d) twinning. Macroscopic strain $E_{11} = 1\%$. Scales multiplied by 10^{-3} for (a) and by 10^{-4} for (b,c,d).

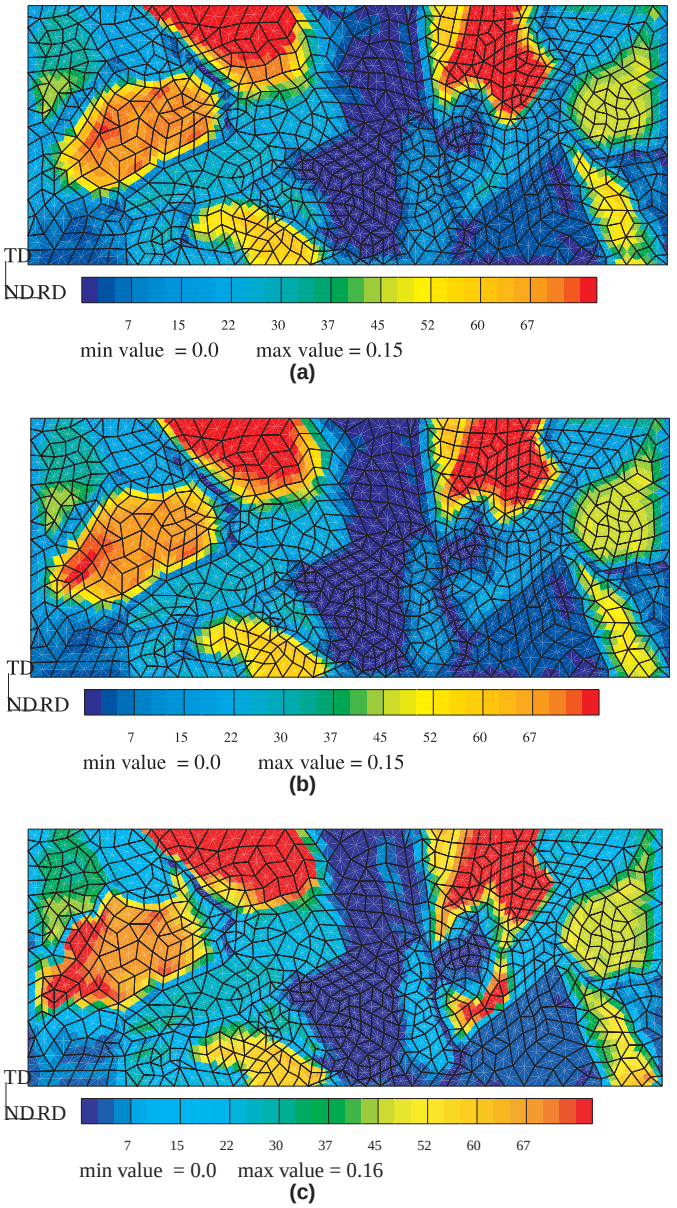

Fig. 10. Plastic strain due to basal slip: (a) section at the interface; (b) mid-section; (c) section at free surface. Macroscopic strain $E_{11} = 1\%$. Scales multiplied by 10^{-3}.

$$\underset{\sim}{\boldsymbol{\varepsilon}}^{p}_{\text{sheet}} \simeq \begin{bmatrix} \varepsilon^{p} & 0 & 0 \\ 0 & -\frac{\varepsilon^{p}}{2} & 0 \\ 0 & 0 & -\frac{\varepsilon^{p}}{2} \end{bmatrix}, \quad \left\langle \underset{\sim}{\boldsymbol{\sigma}}_{\text{grain}^{11}} \right\rangle \simeq \begin{bmatrix} \sigma & 0 & 0 \\ 0 & -3.1\sigma & 0 \\ 0 & 0 & 0 \end{bmatrix} \tag{6}$$

with a strong compressive component on the transverse direction given by the simulation (Fig. 12). This biaxial stress state leads to the activation of non-basal slip systems.

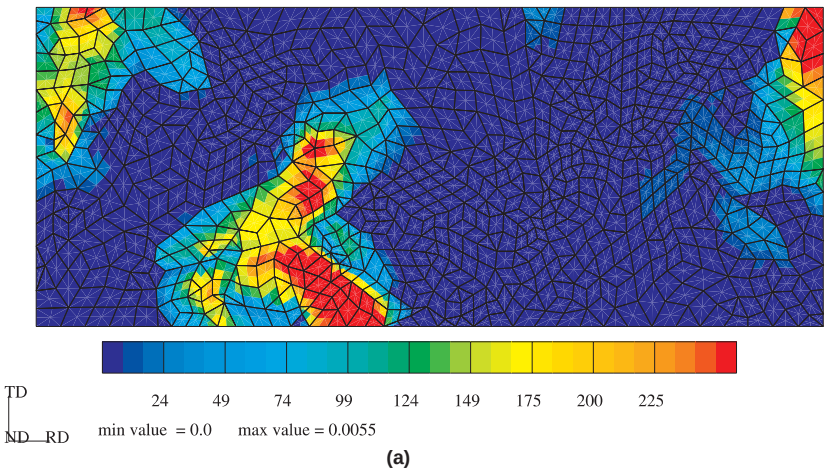

(a)

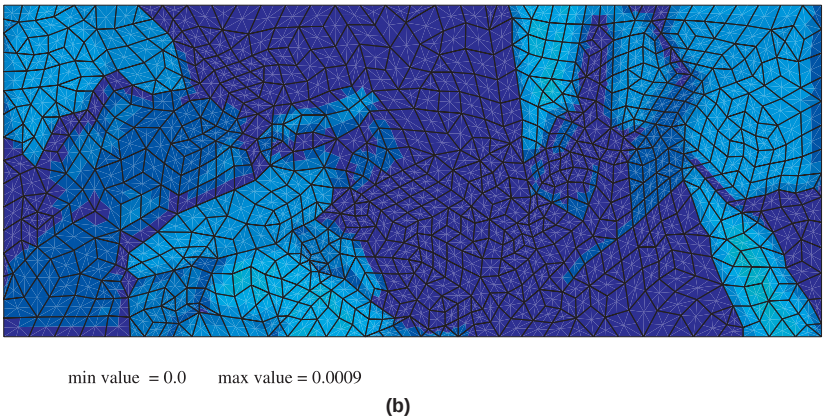

(b)

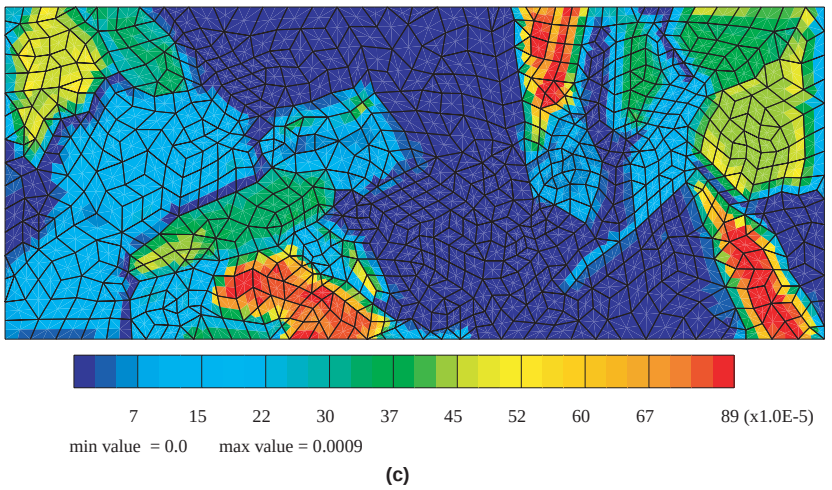

(c)

Fig. 11. Influence of the substrate on the basal plastic strain of the coating. Macroscopic strain $E_{11} = 0.05\%$. (a) without substrate – color scale A; (b) with susbtrate – color scale A; (c) with substrate – color scale B. See the text in Section 4.5. Scales multiplied by 10^{-5}.

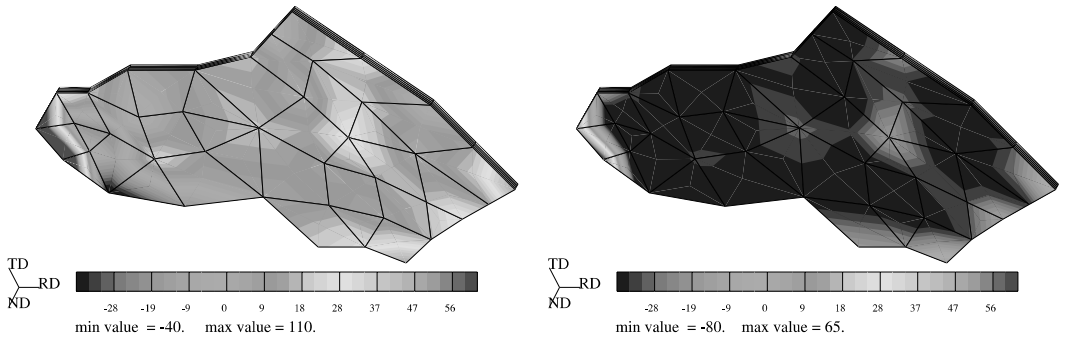

Fig. 12. Stress state on the grain 11 with a substrate.

4.6. Stresses at the interface

One may be interested in delamination process which may be related to normal stresses σ_{33} and shear stresses in the plane of the interface. The computation shows that most of the grains have a slight stress component σ_{33} and non-zero values are localized in the vicinity of grain boundaries. The coating is too thin for a normal stress gradient to develop between the free surface ($\sigma_{33} = 0$) and the interface. In contrast, shear stresses at the interface are quite homogeneous at grain scale, as shown on Fig. 13. Some of the grains exhibit a shear stress of about 20 MPa. The undamaged interface experimentally observed suggests that this value remains weak compared with the cohesive energy of the interface.

4.7. Comparison with experiment

Fig. 14 shows the global mechanical responses load vs. macroscopic strain for the experiment and for the simulation of the galvanized steel sheet. The presence of a thin layer does not significantly affect the global response of the tension of the substrate. The differences are mainly due to the measurement errors for such a small sample. Comparison at the local level is restricted to the evidence of intergranular cracking observed experimentally in Fig. 15. This contributes to the strain accommodation and this may relax the stress

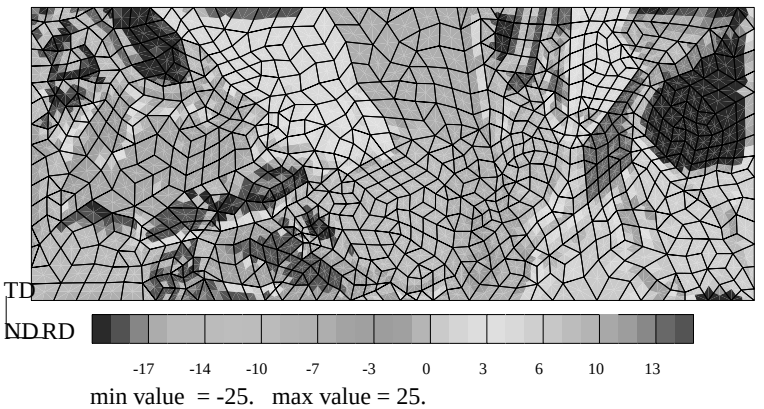

Fig. 13. Shear stress state σ_{12} at the interface.

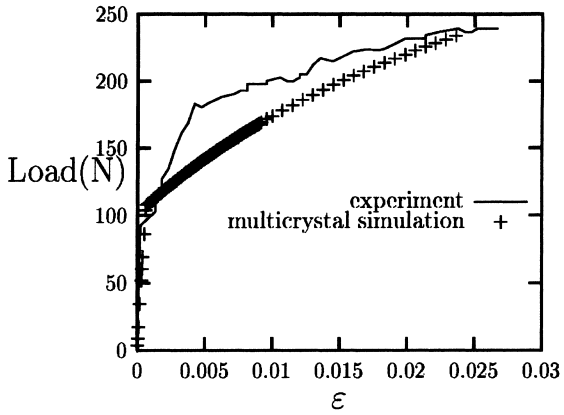

Fig. 14. Global mechanical responses of experiment and substrate + coating FE simulation.

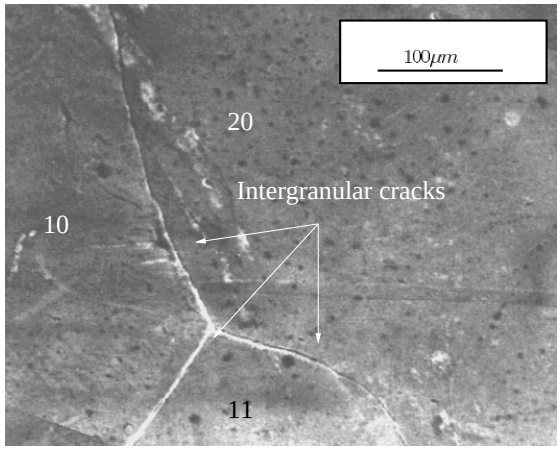

Fig. 15. Intergranular cracks observed on the experiment. Grains 10, 11 and 20 (see Fig. 8 to localize these grains).

concentrations at grain boundaries arising in the FE simulations. This mechanical behavior at grain boundaries on this kind of coating was also observed by Lietzau and co-workers [2]. Evidence of plastic slip in the grain is difficult to detect because of the presence of an unwanted hydroxide layer.

5. Conclusions and future work

The mechanical behavior of a flat multicrystalline zinc coating on a galvanized steel sheet was simulated. The 3-D FE mesh was obtained after experimental characterization of the gauge length of an in situ tensile specimen for the SEM. Special attention was paid to the identification of material parameters for pure and alloyed zinc from literature data (viscosity, CRSS and their evolution). Four slip and twinning system families were taken into account and the importance of interaction between them was underlined. The average crystallographic orientation of the grains was included in the modeling.

The results show that plastic strain of the coating is mainly due to basal slip, even though non-basal slip also occurs in the vicinity of grain boundaries. Experimentally observed stress relaxation phenomenon at grain boundaries is compatible with this result. The coating thickness (10 μm) seems to be too small for significant strain and stress gradients to develop from the interface to the free surface, at the early stage of deformation. The constraining effect of the substrate has been proved to lead to strongly biaxial stress states in the zinc grains.

Further work is necessary to confirm the main features of the deformation of zinc coatings explored in this work. This would include, on one hand, FE simulations with a finer mesh for larger strain levels and different loading conditions (expansion ...), and on the other hand, a systematic experimental approach to determine locally activated slip systems and derive strain maps at the grain levels using strain field measurement techniques. Material parameters of alloyed zinc will be experimentally identified by analysis of mechanical tests performed on a bulk zinc material provided by USINOR.

Acknowledgements

This work is supported by USINOR.

Appendix A. Identification of latent hardening

The hardening law, i.e., the evolution of CRSS with plastic slip, is given by

$$\tau_c^s = \tau_{0c}^s + \sum_{r=1}^{N} Q^s H_{rs}\left(1 - \exp[-b_r \gamma_{\text{cum}}^r]\right), \tag{A.1}$$

where N is the total number of slip systems, including basal and non-basal ones, γ_{cum}^r is the cumulative plastic slip (see Eq. (1)), and H_{rs} is the interaction matrix. This matrix accounts for interaction between slip systems belonging to the same family, but also for interaction between slip systems of different slip system families. An idealized form of the matrix is:

$$[Q^s H_{rs}] = \begin{array}{c} \\ basal \\ prism \\ \pi_2 \\ \vdots \end{array} \begin{array}{c} \begin{array}{ccc} basal & prism & \pi_2 \end{array} \\ \begin{pmatrix} Q^{\text{b}}\begin{pmatrix} \mathbf{h}_1^{\text{b}} & \mathbf{h}_2^{\text{b}} & \cdots \\ \mathbf{h}_2^{\text{b}} & \mathbf{h}_1^{\text{b}} & \cdots \\ \mathbf{h}_2^{\text{b}} & \mathbf{h}_2^{\text{b}} & \ddots \end{pmatrix} & \mathbf{Q}^{\text{b}} h_{\text{p}}^{\text{b}} & \mathbf{Q}^{\text{b}} \mathbf{h}_{\pi_2}^{\text{b}} & \cdots \\ Q^{\text{p}} h_{\text{p}}^{\text{b}} & Q^{\text{p}}\begin{pmatrix} h_1^{\text{p}} & h_2^{\text{p}} & \cdots \\ h_2^{\text{p}} & h_1^{\text{p}} & \cdots \\ h_2^{\text{p}} & h_2^{\text{p}} & \ddots \end{pmatrix} & Q^{\text{p}} h_{\pi_2}^{\text{p}} & \cdots \\ \mathbf{Q}^{\pi_2} \mathbf{h}_{\pi_2}^{\text{b}} & \mathbf{Q}^{\pi_2} h_{\pi_2}^{\text{p}} & \mathbf{Q}^{\pi_2}\begin{pmatrix} h_1^{\pi_2} & h_2^{\pi_2} & \cdots \\ h_2^{\pi_2} & h_1^{\pi_2} & \cdots \\ h_2^{\pi_2} & h_2^{\pi_2} & \ddots \end{pmatrix} & \cdots \\ \vdots & \vdots & \vdots & \ddots \end{pmatrix} \end{array} \tag{A.2}$$

Bold letters of the matrix of Eq. (A.2) were identified from literature data. The diagonal terms of the submatrices are called self-hardening coefficients, whereas the out-of-diagonal terms correspond to latent hardening. The coefficient h_i^s is dimensionless and Q^s has the dimension of stress. Edwards and Washburn [19] worked on latent hardening of basal system in zinc and the interpretation of their results leads to the following values: $Q^{\mathrm{b}} \equiv 1$ MPa, $b_{\mathrm{b}} \equiv 3$, $h_1^{\mathrm{b}} \equiv 1$, $h_2^{\mathrm{b}} \equiv 2$. These values are consistent with the experimental results provided by Stofel and Wood [10] and by Bosin et al. [14]. Using respectively tension/torsion tests on single crystals and compression tests on bicrystals, the latter authors have studied the latent hardening for pyramidal π_2 slip and the interaction between basal and pyramidal π_2 slips. Parameters were identified to be: $Q^{\pi_2} \equiv 15$ MPa, $b_{\pi_2} \equiv 30$, $h_1^{\pi_2} \equiv h_2^{\pi_2} \equiv 1$ and $h_{\pi_2}^{\mathrm{b}} \equiv 2.8$. Latent hardening for prismatic slip system was calculated assuming that it has a similar behavior as basal and pyramidal π_2 slip systems, i.e., $Q^{\mathrm{p}} \simeq \tau_c^{\mathrm{p}}$, $b_{\mathrm{p}} \simeq 10$, $h_1^{\mathrm{p}} \equiv h_2^{\mathrm{p}} \simeq 1$. No latent hardening was assigned to twinning.

References

[1] S. Lazik, C. Esling, J. Wegria, Cracking in zinc layers on continuous galvanized steel sheets, Textures and Microstructures 23 (1995) 131–147.

[2] J. Lietzau, M.J. Philippe, C. Esling, J. Wegria, M. Dubois, Pre-cracking and cracking of zinc coated steel sheets during deformation, in: F.E. Goodwin (Ed.), Zinc-based Steel Coating Systems, T.M.S, 1998, pp. 207–217.

[3] C. Maeda, J. Shimomura, H. Fujisawa, M. Konishi, The structure and deformation behavior of hot-dip galvanized coatings, Scr. Metall. 35 (1996) 333–338.

[4] W.D. Nix, Yielding and strain hardening of thin metal films on substrates, Scr. Mater. 39 (1998) 545–554.

[5] C. Lineau, P. Viaris de Lesegno, C. Rey, T. Chauveau, Evolution of the local strain field and local crystallographic rotation field in grains of steel polycrystals, in: J. Ziebs, J. Bressers, H. Frenz, D.R. Hayhurst, H. Klingelhoeffer, S. Forest (Eds.), Symposium on Local strain and temperature measurements in non-uniform fields at elevated temperatures, Woodhead Publishing Limited, 1996, pp. 159–167.

[6] R. Becker, Effects of strain localization on surface roughening during sheet forming, Acta Mater. 46 (1998) 1385–1401.

[7] R. Becker, S. Panchanadeeswaran, Effects of grain interactions on deformation and local texture in polycrystals, Acta Mater. 43 (1995) 2701–2719.

[8] A. Staroselsky, L. Anand, Inelastic deformation of polycrystalline face centered cubic materials by slip and twinning, J. Mech. Phys. Solids 46 (1998) 671–696.

[9] P.G. Partridge, The crystallography and deformation modes of hexagonal close-packed metals, Met. Rev. 12 (1957) 169–194.

[10] E.J. Stofel, D.S. Wood, Fracture of zinc single crystals, in: Fracture of solids, Metal. Soc. Conference, (Ed.), 21–24 August 1963, vol. 20, pp. 521–539.

[11] R.L. Bell, R.W. Cahn, The dynamics of twinning and the interrelation of slip and twinning in zinc crystals, Proc. Roy. Soc. A 239 (1956) 494–520.

[12] R.C. Pond, Symmetry in Science and Art, Plenum Press, 1991.

[13] K.H. Adams, T. Vreeland Jr., Impurity effects on basal dislocation in zinc single crystals, Trans. Metall. Soc. AIME 242 (1968) 132–139.

[14] M.E. Bosin, F.F. Lavrentev, V.N. Nikiforenko, Localization of plastic deformation in zinc crystals containing forest dislocations, Phys. Solid State 38 (1996) 1972–1975.

[15] J.J. Fundenberger, M.J. Philippe, F. Wagner, C. Esling, Modelling and prediction of mechanical properties for materials with hexagonal symmetry (zinc, titanium and zirconium alloys), Acta Mater. 45 (1997) 4041–4055.

[16] B. Mikulowski, The effect of the prestrain temperature on the hardening of Zn and ZnGa monocrystals on the $(0001)\langle 11\bar{2}0\rangle$ system, Phys. Stat. Sol. 157 (1996) 287–292.

[17] D. Stahl, H. Margolin, Pyramidal flow stress of single crystal zinc, Acta Mater. 32 (1984) 1817–1823.

[18] ASM, (Ed.), Metal Handbook, vol. 9, Metallography and Microstructures, 1985.

[19] E.H. Edwards, J. Washburn, Strain hardening of latent slip systems in zinc crystals, Trans. Metall. Soc. AIME 200 (1954) 1239–1242.